TNO TPD Contributions to High Precision Optical Metrology, a Darwin Metrology Breadboard for ESA

Adrianus L. Verlaan[a], Teun C. van den Dool[a], Ben C. Braam[a], Bertrand Calvel[b], Rainer Sesselman[c], Wolfgang Pöschel[d], Denys Dontsov[d], Isabel Cabeza Vega[e], Eberhard Manske[f], Thilo Schuldt[c], Zoran Sodnik[g]

[a]TNO TPD Institute of Applied Physics, Stieltjesweg 1, Postbus 155 2600AD Delft, The Netherlands
[b]EADS ASTRIUM, 31av. Des cosmonautes, Z.I. du Palays, 31402 Toulouse Cedex 4, France
[c]EADS ASTRIUM, An der Bundesstrasse 31, 88039 Friedrichshafen, Germany
[d]SIOS Meβtechnik, Am Vogelherd 46, D-98693 Ilmenau, Germany
[e]EADS CASA Espacio, Ava. de Aragon, 404, 28022 Madrid, Spain
[f]TU Ilmenau, Fakultät Maschinenbau, Am Ehrenberg, PF 100565, D-98684 Ilmenau, Germany
[g]ESA ESTEC, Keplerlaan 1, Postbus 299, 2200 AG Noordwijk, The Netherlands

ABSTRACT

A Darwin precursor breadboard, comprising both fine lateral and longitudinal metrology sensors was designed, built and partially tested. The lateral metrology sensor was designed and built by TNO TPD and more than meets the imposed requirements. The longitudinal metrology sensor consists of a dual wavelength interferometer with an integrated delay line for optical path stabilisation. Here TNO TPD supplied the delay line and implemented the optical path difference stabilisation control. Experiments under ambient conditions show that noise reduction up to five orders of magnitude is achievable.

Keywords: Darwin metrology, OPD-stabilisation, Delay line.

1. INTRODUCTION

The Darwin baseline configuration consists of six flyers equipped with telescopes. These flyers fly in hexagonal configuration around a central hub satellite. The collected stellar and planetary light is recombined in the hub and used either for high-resolution imaging or nulling, where the starlight interferes destructively, enabling the light from the planet to be observed.

The formation flying with these satellites requires a longitudinal resolution of the optical path difference (ODP) far below a wavelength, whereas the absolute distance (between 25 m and 250 m) should be known as accurate as 70 microns. Lateral resolutions of several tens of microns are required to guarantee sufficiently accurate beam overlap. The metrology required, to show that formation flying and OPD-stabilization with this type of accuracies is feasible, was bread boarded for ESA. This system consists of two sensors. The first is the Dual Wavelength Interferometer, which is stabilized on an Iodine absorption line, and which is used for both absolute and relative longitudinal measurements. In the optical path a delay line is positioned to allow accurate OPD-stabilization. The second sensor is the Fine Lateral Sensor, which is based on a collimated beam on a position sensitive device (PSD). This sensor facilitates the accurate flyer position control, required for beam overlap in the hub. A third sensor, the Frequency Sweeping Interferometer, which is used for absolute longitudinal measurements, although required, is not discussed, since it hasn't been bread boarded by TNO.

Topics to be presented include a brief introduction to the Darwin formation flying metrology and the major error contributions. The optical scheme of our breadboard system will be presented. Finally the (preliminary) experiments will be discussed.

2. METROLOGY REQUIREMENTS

The DARWIN project is dedicated to spectroscopic measurement on the planetary atmospheres of nearby stellar systems. Here the main objective is to detect gases that could indicate life. Within the DARWIN project a set of free flying satellites, equipped with telescopes, is used as aperture synthesis system. By tuning the base length (satellite separation) and adding a half wave phase change between the combining beams, it is feasible to let the starlight interfere destructively, whereas the planetary light interferes constructively. This application is the so-called nulling interferometry. This new field of satellite application imposes a very stringent set of requirements onto the metrology system. Calvel et al.[1] describes the required technology and most recent status of the requirements for the various sensors. Here only a brief summary of the required metrology and the imposed requirements are given.
The DARWIN telescopes are operated using a base length (telescope separation) of 50m to 500m. These values are typical in order to achieve the required 0.1 arcsec angular resolution, which is determined by the most nearby Earth-Sun like configurations. Within this operating range the actual telescope distances should be known with 70 μm accuracy, whereas the arms of the interferometer should be kept equal within 5 nm/√Hz. Since it is hard to guarantee the latter by satellite attitude control, an optical delay line is added in the optical path. Here the relative optical path is measured using an interferometer, and the data is used to stabilise the optical path difference (OPD) between the telescope beams. Due to the complexity of the metrology system ESA has initiated the "High Precision Optical Metrology" (HPOM) project. Here the main objective is to breadboard and study the main metrology systems for a simplified DARWIN precursor mission (Presumably SMART 3). On this breadboard three sensors were planned, being the Dual Wavelength Interferometer (DWI) with delay line and OPD-control, the Fine Lateral Sensor (FLS) and the Frequency Sweeping Interferometer (FSI). Since the last was tested separately, only the first two sensors were implemented on the breadboard. In the HPOM experiments the following requirements are required:
The system operates under vacuum conditions, and has the capability of being used for any distance between 25 m and 250 m and with an operation frequency of 10 Hz. For the relative longitudinal metrology an accuracy of 2 nm/√Hz is required, whereas the Lateral metrology accuracy should meet 10 μm/√Hz within a working range of ±5 mm. The absolute longitudinal metrology requirement is ±70 μm. Finally the OPD should be stabilised within 5 nm RMS.

3. LATERAL DISPLACEMENT USING FINE LATERAL SENSOR

The Fine Lateral Sensor bridges the gap between the required 10 μm/√Hz accuracy and the few mm accuracy delivered by the Course Lateral Sensor. Within a ±5 mm range any point can be taken as the starting position. Around this set point the sensor is used as a nul sensor and it should indicate the direction of lateral displacement. Therefore it is not the sensor linearity that is important, but the sensitivity over the capture range and the stability during the many hours operation time.

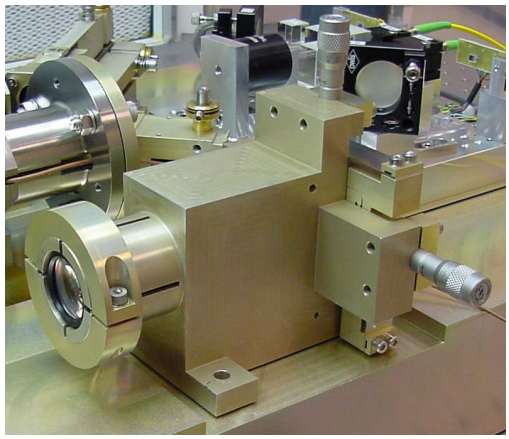

Figure 1 Fine Lateral Sensor side view, showing lens 4-spring mounting

The optical design is based on a light emitting collimated source on one of the satellites and a position sensitive detector on the second satellite. Due to the fact that the flyers show the best pointing stability, the source is placed in the flyer and the detector in the hub. The optical source consists of Super Luminescent Diode (SLD) a single mode fibre and a focusing lens. Here the design was determined by the wish to have a roughly constant spot size over the entire working range and by the imposed stability. The selected SLD is operated around a wavelength of 820 nm. This choice is based on SLD and fibre availability and being far away from metrology laser. The SLD light source is fibre coupled allowing thermal decoupling from the actual breadboard. An additional advantage of the single mode fibre is the extremely small dimension of the emitting surface. This allows a small beam divergence using only a small optical system. The FLS beam diameter is chosen to be 22 mm with the shape of a truncated Gaussian beam. To focus the beam in a spot at 250 m a commercial air spaced doublet was selected. Due to diffraction and geometrical aberrations the light spot at the end of the working range is approximately the same size and is dominated by diffraction. In the intermediate range the beam shape will change slowly from truncated Gaussian to the Airy diffraction pattern.

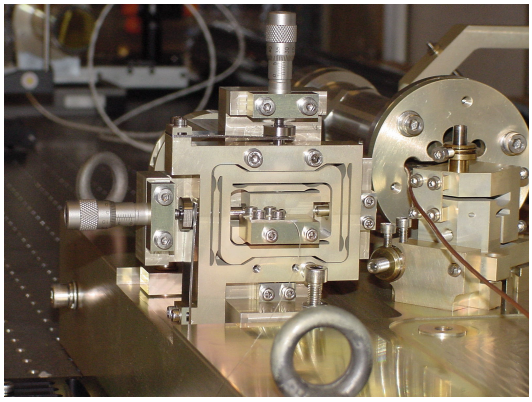

Figure 2 Fine Lateral Sensor rear view, showing flexure fibre adjustment mechanism

For the optimisation for stability of the emitter assembly, both the spot position on the detector and the emitting angular distribution are required to be stable. Any change over time will be falsely interpreted as a satellite movement. By using a single mode fibre, the light spot angular distribution has become a material and geometry property and therefore is likely to be very stable. The pointing of the entire source assembly is required to be stable within 40 nrad. Over the 250 m working range this angular error would be interpreted as a 10 μm satellite displacement. Due to the small dimensions of the source this 40 nrad requirement implies the relative alignment between fibre and lens to remain stable within 4 nm. This extreme stability can only be achieved by a proper mechanical design and stringent temperature stability requirements.

Although it is foreseen that during operation in space stray light reduction is required, it has not been implemented in the experimental breadboard. In space operation there are two types of stray light sources that can be identified. A first is stray light caused by internal sources, meaning metrology lasers and the science light. A second source of stray light is the presence of external sources like stars. Since all the internal sources are aimed at positions close to the receiver, from a large distance. Beam divergence and scattering of light on optical elements and just will cause light to be directed onto the FLS-detector. Here apertures and baffles will be useless. It is foreseen that spectral filtering and modulation of the source light, which allows AC-detection, will be used.

The mayor mechanical design drivers for the FLS are the temperature stability, vacuum compatibility and lowest complexity. These requirements result in the use of Aluminium, high symmetry and a low number of elements. The optical design of the FLS consists of two elements, a glass fibre and a lens assembly. These elements need to be adjusted with respect to each other in three directions. Other adjustments such as the rotation of the fibre or the rotation of the lens assembly can be avoided by mounting them with sufficiently strict tolerances. The resulting adjustments are the fibre position adjustment, which is performed using a flexure and the focussing, which is performed by sliding the lens assembly back and forth. The lens assembly is mounted using a tight 4-spring guiding. The lens assembly is clamped in between the springs and can be slided back and forth. Using a circular clamp around the 4 springs the position is locked. By using this symmetrical design any thermal expansion will be around the optical axis and therefore have no effect on the critical relative lateral position.

The fibre adjustment mechanism is based on flexure in two directions. Again this mechanism has been selected to guarantee the highest degree of stability on the fibre position. Experiments on several mechanisms have shown that a flexure shows the least creep after locking. Also a flexure only allows two directions of movements All other movements of the fibre tip are avoided due to the high stiffness of the flexure plate in these directions. The flexure is preloaded with two springs resulting the double range of movement. The actual adjustment is performed using micrometer screws. The locking of the position is performed using aluminium spriets. These are mounted directly into the centre part and are clamped onto the sensor body. After locking the adjustment screws are removed.
The FLS performance was assessed during preliminary experiment under ambient conditions at TNO TPD. Although vacuum equipment and experimental facilities are available, no vacuum experiments were performed. The project partner EADS CASA in Madrid is currently performing these experiments. In the preliminary experiments not only the sensitivity, but also the pointing stability was determined. These test show that the resolution requirement of 10 μm/√Hz is easily met, also for control frequencies up to 1kHz. At the control bandwidth of 10 Hz, 0.2 μm resolution has been achieved. .

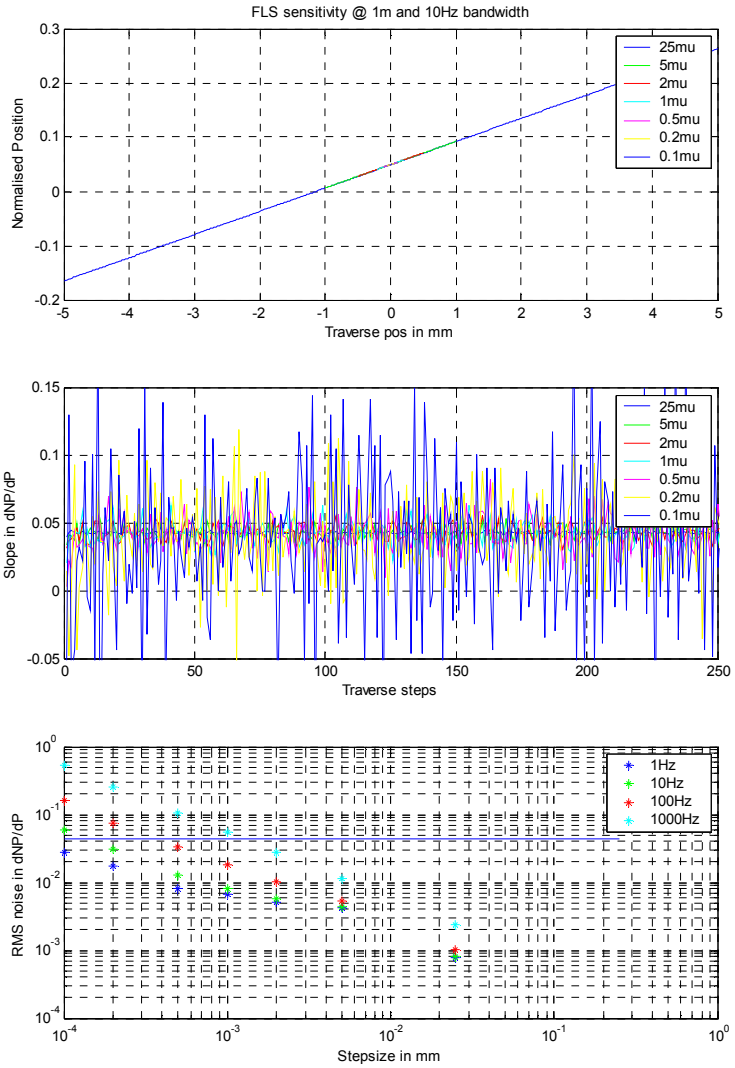

Figure 3 Fine Lateral Sensor sensitivity.

In figure 3 the sensor response over a large position range variation is shown. In the first plot the actual sensor response is given, whereas the second plot depicts the slope of the data. During this experiment the position step size was varied from 0.1 μm to 25 μm. As can be observed the sensor response is close to linear over the entire scan range. This is probably due to the well-confined beam shape at this short distance of 1 m. At larger separation distances some non-linearity might show up. The second plot of figure 3 shows that for each position within the scan range, the sensitivity is sufficient to distinguish each step, for steps larger than 0.5 μm. Keep in mind that the first and second plots only depict data at 10 Hz sampling bandwidth.
In the third plot the sampling bandwidth is varied from 1 to 1000 Hz. For each combination of sampling bandwidth and step size the standard deviation of the slope is given. Additionally a line with the required resolution is depicted.

The variation of temperature and its effect on the FLS pointing is estimated using a 5 m focal length telescope. (Delft Test bench Interferometer)[2] See figure 4. Here the FLS beam is directed into the telescope together with a reference beam. Both beams are focussed on a digital camera. A computer monitors the spot positions during the experiment.

.

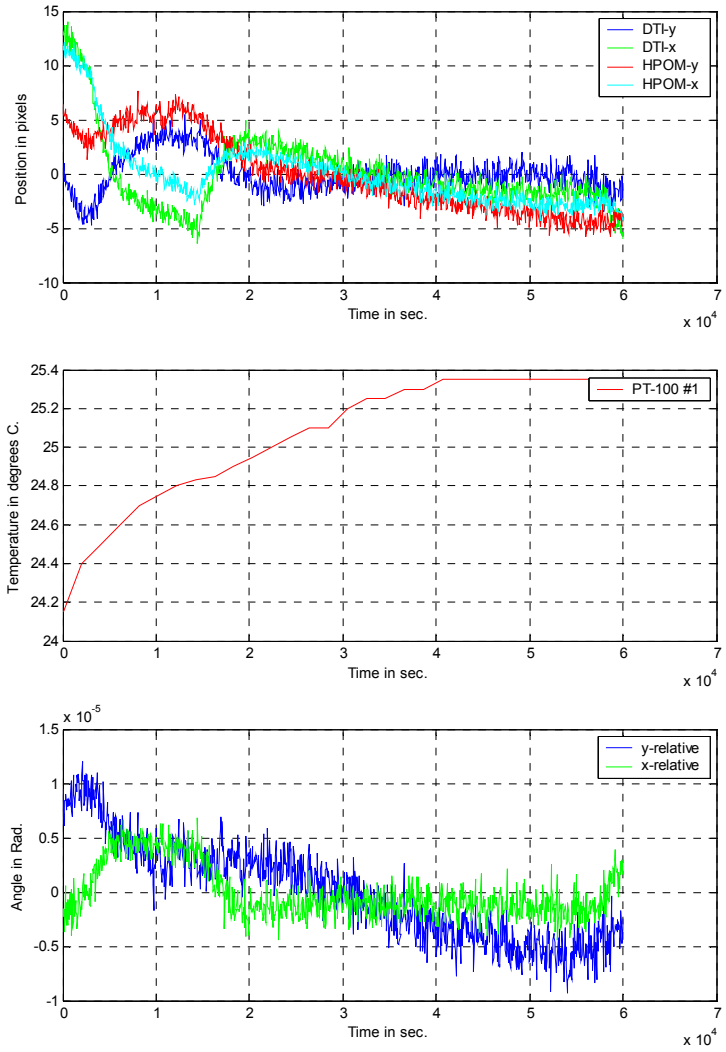

Figure 4 Fine Lateral Sensor angular stability

The first plot in figure 4 depicts the spot positions as a function of time. The average pixel position was removed. As can be observed, the drift during the experiment is similar for both beams. Both x-components have the same curve shape and nearly the same amplitude. The y-components show the same features, but they slowly drift away from each other. This effect probably is introduced by the different heights at which the beams are introduced into the system. A change in temperature directly results in a shift of the camera position and thus in the measured angle. Consequently the common behaviour should be neglected when regarding the FLS-stability. This will be hard due to the difference in amplitudes.
In the second plot the temperature on top of the FLS body is shown. During the night this temperature stabilises around 25.3°C. The measurement noise has been removed from the data to improve the clarity.
In the third plot the pixel data is translated to variation of pointing. Here only the relative changes between DTI and the FLS are shown. Most of the variations take place between 16:00 hrs and 21:00 hrs. (The first 18000 seconds.) After this time the DTI stabilises whereas only one of the FLS directions stabilises. During the night the x-drift is less than 1 μrad, whereas the y-drift is as large as 8 μrad.
The measured drifts are substantially larger than the angular stability budget for space conditions, but acceptable for experiments. The largest difference found in the experiment is about 14mrad where the temperature fluctuated about 1.2°C. The SMART requirement is that the drift on the detector is less than 20 μm, which corresponds to an angle of 80 nrad. Assuming the drift is proportional to the temperature, the temperature should be maintained within 7 mK to achieve the stable pointing. Predictions yield 4 mK as the required value. An additional remark is that a substantial part of this error is introduced by the measurement method and not by the FLS. When regarding the CASA experiments with an assumed optical path of 10 m, the temperature should be kept within 0.17 K. Again this value is larger than the assumed 0.1 K temperature stability in DARWIN. Some critical remarks are justifiable here. The period over which the stability is monitored is less than a temperature cycle of 24 hours. A measurement over more cycles would yield a better understanding of the behaviour. Secondly only one PT-100 is used. Therefore only one local temperature is monitored. Still the results are promising.

4. LONGITUDINAL METROLOGY USING DUAL WAVELENGTH INTERFEROMETER

All longitudinal metrology on the breadboard is based on the Dual Wavelength Interferometer (DWI). This interferometer is designed and supplied by SIOS Meβtechnik GmBh. The DWI consists of two integrated interferometers with coinciding optical paths but with a slightly different wavelength. Each of the interferometers can be used for relative measurements, whereas the combination yields absolute distance information over the created synthetic wavelength. Due to the long working range of 250m the laser frequency has to be stabilised to 10^{-12} in order to meet the 2.5nm relative accuracy. For this purpose an Iodine vapour cell is used as an external frequency reference.

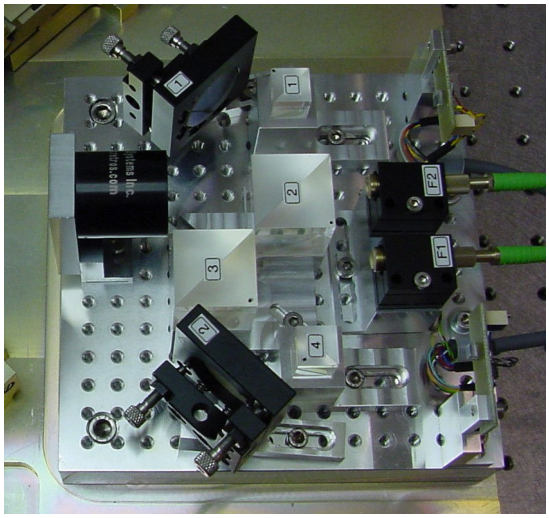

Figure 5 Interferometer head, showing the fibre collimators, polarising beam splitters, reference retro reflector, the fold mirrors and the two detectors.

The DWI can be divided into two parts, a first part which is placed outside the vacuum whereas a second part is placed inside the vacuum tank. The part inside the vacuum is the actual interferometer head. All other hardware, from laser to phase meters and controller are placed outside the vacuum. Of course this type of components can be adapted for vacuum use. However at this stage of the DARWIN project this wouldn't provide a substantial amount of useable extra information.

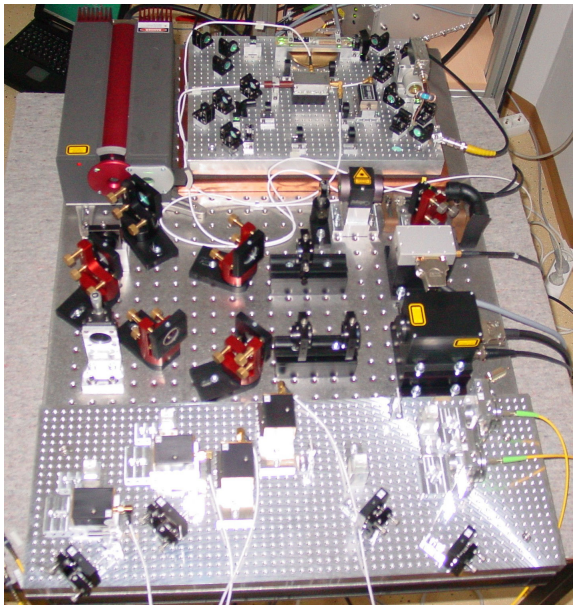

Figure 6 Interferometer breadboard, comprising two laser sources, frequency stabilisation breadboard and frequency modulation breadboard

In figure 6 the DWI system part outside the vacuum is depicted. Here the four main subsystems can be identified. These are the laser sources (diode pumped continuous YAG), the frequency stabilisation breadboard, the laser frequency coupling between the two lasers and the interferometer breadboard with AOM's and fibre coupling. Here the set-up is explained briefly since it is utilised for the OPD-stabilisation. For a more comprehensive explanation the reader is referred to Calvel et al.[1] or the subsystem manufacturers.

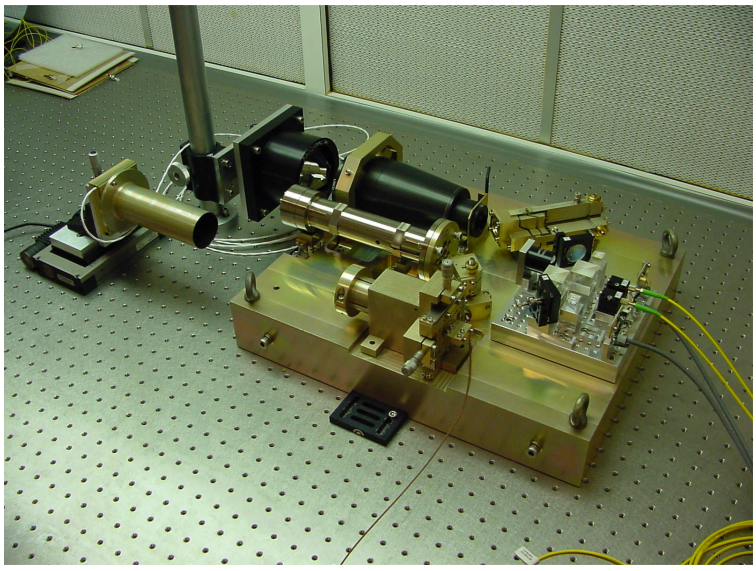

Figure 7 HPOM breadboard (on clean bench), comprising FLS source and detector, the interferometer head, the delay line, fold mirrors, the beam expander and the large diameter external retro reflector.

In figure 7 the HPOM breadboard inside the vacuum is depicted, which is designed by TNO TPD. Here the two main subsystems can be identified. These are the FLS and the longitudinal metrology system comprising the interferometer head (designed and produced by SIOS), the delay line, the fold mirrors and a beam expander. All components (except the delay line) are made of aluminium because of the high thermal conductivity and to avoid material pairing problems. The interferometer head in its turn consists of two fibre collimators, four polarising beam splitters, two fold mirrors, a reference corner cube and the two detectors. The emitted light from each fibre is split in to a measurement and a reference arm and then send to the two detectors. One measurement arm consists of the reference corner cube, whereas the second arm is led through the delay line, fold mirrors, beam expander and towards the large external corner cube. Changes in the optical path are measured as phase changes between the two detector signals.
The two folding mirrors on the HPOM breadboard are a course angular adjustment assembly and a fine angular adjustment assembly. The first mirror directly behind the delay line is used to position the light spots at the beam expander entrance, whereas the second mirror is used to point the interferometer beam. The actual mirrors consist of zerodur substrates ($\lambda/20$) with a protected silver coating. Due to the high stability requirements a monolithic flexure adjustment mechanism was selected. These mirrors have successfully been applied in various experiments, amongst which the GAIA measuring set-up, where a picometer sensitivity has been achieved.
A beam expander is required to expand the beams from 4 mm diameter to a minimum of 23 mm to meet the required operating distances without too large power losses. Here a commercial 9-times magnification laser beam expander with large aperture (12 mm) was selected. Consequently the beam diameter between the beam expander and corner cube will be as large as 36 mm. To increase the stiffness an additional support is anticipated. The unit will be mounted on the c-mount thread and two adjustable cams will support the units' front side. The optical performance of this device is not specified. During experiments it was identified that the spot quality in the outer half of the aperture is low. This in turn results in a reduced contrast on the interferometer detector.
The external corner cube that should be mounted on the second satellite is required to be as large as 3-inch. The PROSystems 3-mirror retro reflector is provided by SIOS and mounted separately on the optical table.

5. OPTICAL PATH STABILISATION USING A DELAY LINE

For the stabilisation of the optical path on the HPOM breadboard a delay line is used. This delay line is based on an OAST (Optical Aperture Synthesis Technology) delay line where a few mechanical modifications have been made. First of all the mechanical interfacing is modified and simplified. Secondly the delay line has been adapted for vacuum use. It has been cleaned and all screws have been equipped with spring rings to facilitate outgassing. The PI-820 low voltage piezo can be used above 0.1 bar or below 0.1 mbar. In between these pressures another piezo element should be selected. The OAST delay line is a 2-stroke delay line with an optical design based on the cats' eye principle. The delay line consists of two optical elements. The first is a spherical mirror, whereas the second is a small flat mirror, which is mounted directly on the tip of the piezo in the focus of the primary mirror. Moving the secondary mirror back and forth changes the optical path length by twice the mirror displacement. Here the long stroke is not used and has been removed to simplify the design. The resulting optical stroke of the delay line is ±30 μm, which is more than required here.
Variations in the optical path can be compensated by adjusting the piezo length in the delay line. The OPD is compensated using closed loop control. First the interferometer measures the optical path length through the entire system. This data is transferred to the OPD-control PC. The ODP-controller adjusts the secondary mirror position in the delay line using a piezo actuator. Now a new OPD can be measured. Previously in a TPD laboratory setup, reductions have been established of a factor 1000 (2 μm vibrations reduced to 2 nm RMS with a 2.5nm resolution interferometer). The OPD controller is based on an Intel Pentium PC with a Real-Time Linux operating system. The sampling and control frequency is 5 kHz. The interface with interferometer consists of 32 bit parallel connection where the synchronization is indicated on a separate line by the interferometer. A single analogue 12 bit output is used to transfer the required position data to the piezo amplifier (PI E660) and then the delay line.
Two types of OPD-controllers are implemented here. The first is a classical PID controller and the second is an adaptive IMC-controller. During experiments noise is digitally added to the delay line position data, since the laboratory environment doesn't provide us with sufficient noise to fully test the system. Two types of noise were used to test the OPD control, being a first order drop off and a second order drop off noise. Additionally the integral noise level is varied in the experiments.

This first controller is a classical PID-controller with the three controlling actions P, I and D. The first action gives a proportional response. It sets the correcting signal S proportional to the measured OPD-deviation dZ. The second I is the integrating correction. Here the correcting signal increases as the deviation dZ persists for a longer period. It is proportional to the integral of deviation over time. The last setting D refers to the derivative correction. This component is implemented to stabilise the closed loop control and is proportional to the slope of the signal. One of the main advantages of the PID controller is the well-known behaviour and the controller simplicity, which could be an advantage when being used in space.
The adaptive IMC controller is a more advanced type of algorithm that learns and adapts its settings during operation. The IMC controller takes in to account the presence of modal components in the system response and the shape of the disturbance spectrum. Consequently it will perform better than the classical PID controller in situations where the disturbance spectrum is complex or unknown in advance, where the system contains strong modal components, or where the disturbance spectrum alters in time.
At receipt of a 'control on' command the controller will carry out three actions. These are a calibration sequence, which includes measuring the 'round going' transfer function including the piezo actuator and IFM. Next it will take the 1 second average IFM output as the set point. And then it will stabilise the OPD to the set point until a command 'control-off' is given. In figure 456 the algorithm scheme is depicted.

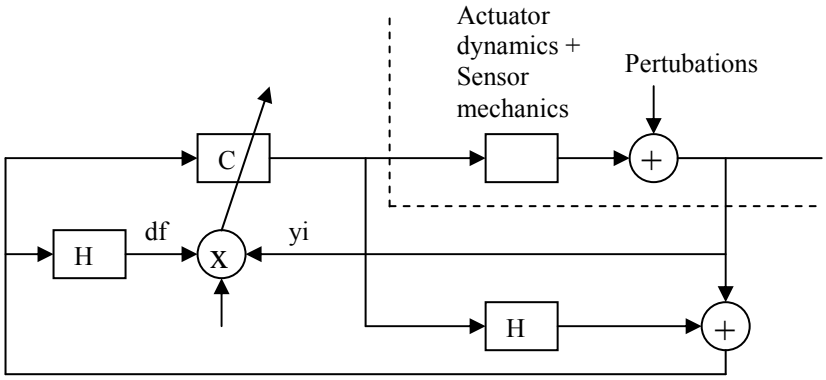

Figure 8 Adaptive IMC controller scheme, showing the data streams during the OPD stabilisation.

H contains the model of the system that is measured at start-up. The complexity of H can be adapted to the complexity of the system. More complexity means that more processing power is needed. In this case the complexity appeared to be low. Also the complexity of the controller C can be adapted to the required system complexity H and the required performance.
The round going delay determines the controller performance to a large extend. Therefore the eigen frequencies and bandwidth of all components should be high and the sampling frequency should be sufficiently large. During all experiments the sampling frequency was 5 kHz.
Several experiments were performed and the results are discussed here. Two OPD-controllers were tested (PID and IMC), the noise type and the noise amplitude have been varied, and the effect of introducing the beam expander (BE) is tested. Although the performance of the bare interferometer is important, it falls out of the TNO scope and therefore it has not been tested here, however its performance is currently under investigation at EADS CASA.

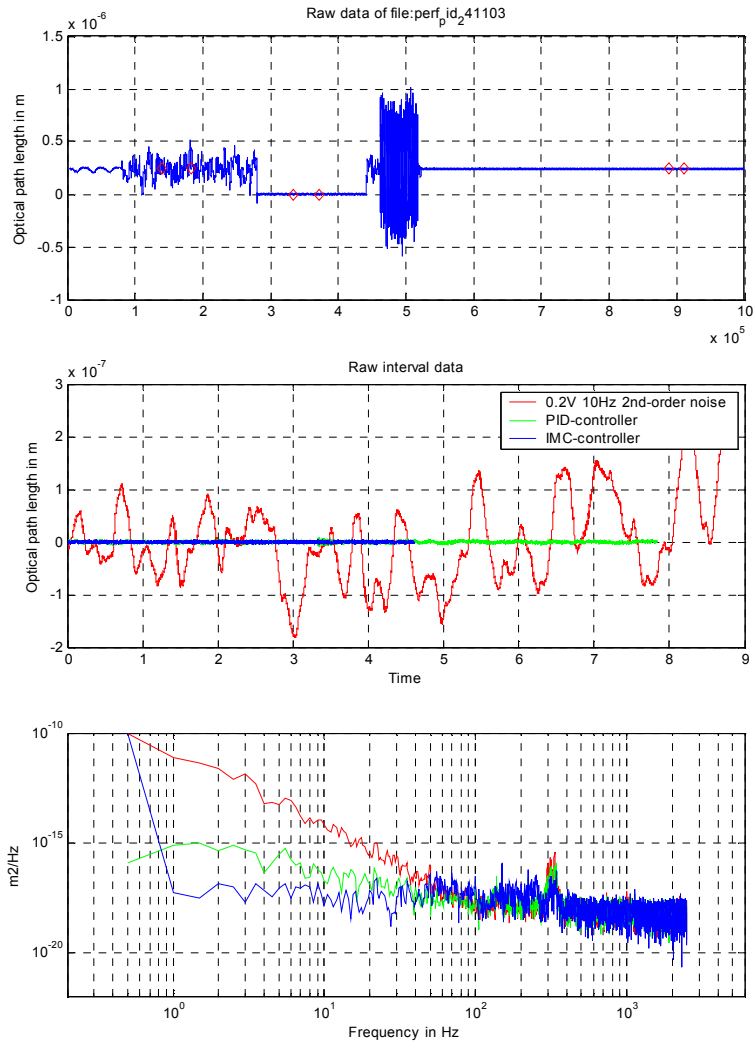

Figure 9 IMC controller versus PID controller performance

Here the IMC and PID controllers are compared. In the first plot of the figure 9 the raw OPD is depicted. The various operation modes are executed sequentially where the red diamonds indicate which parts of the data were selected for analysis. In the first 100000 samples nothing was done, after which the noise introduction for system analysis is started. One clearly observes the increased amplitude of the OPD. At about 280000 samples the PID controller was started. The OPD is adjusted quickly to the set point, which was 0 µm here. Clearly the controller substantially reduces the noise. At about 450000 samples the OPD controller is switched off and the IMC-controller is switched on. The OPD directly changes back to the value of before the PID-controller. The IMC controller starts with a delay, so that the background noise level is observed again. Then the transfer measurement is performed. Using a large amplitude binary noise the response of the OPD is measured. At 520000 samples the measurement is stopped and the IMC-controller started. This status remains until the end of the experiment.
In the second plot the selected data is depicted after subtraction of the mean value. This way a good impression of the OPD behaviour during the various modes of operation is obtained. The noise added in the experiment has an amplitude of 0.2 V on the piezo steering voltage. The noise is based on white noise after which a second order drop off filter has been applied. In the plot the noise results in OPD-changes of about ±200 nm.

In the third plot the power spectral density (PSD) is depicted to show the spectral performance of the controllers. As can be seen both controllers work in the 0 Hz to about 50 Hz, where the reduction is better for lower frequencies. For frequencies over 50 Hz no reduction is obtained. The Piezo amplifier unit induces this cut-off frequency.

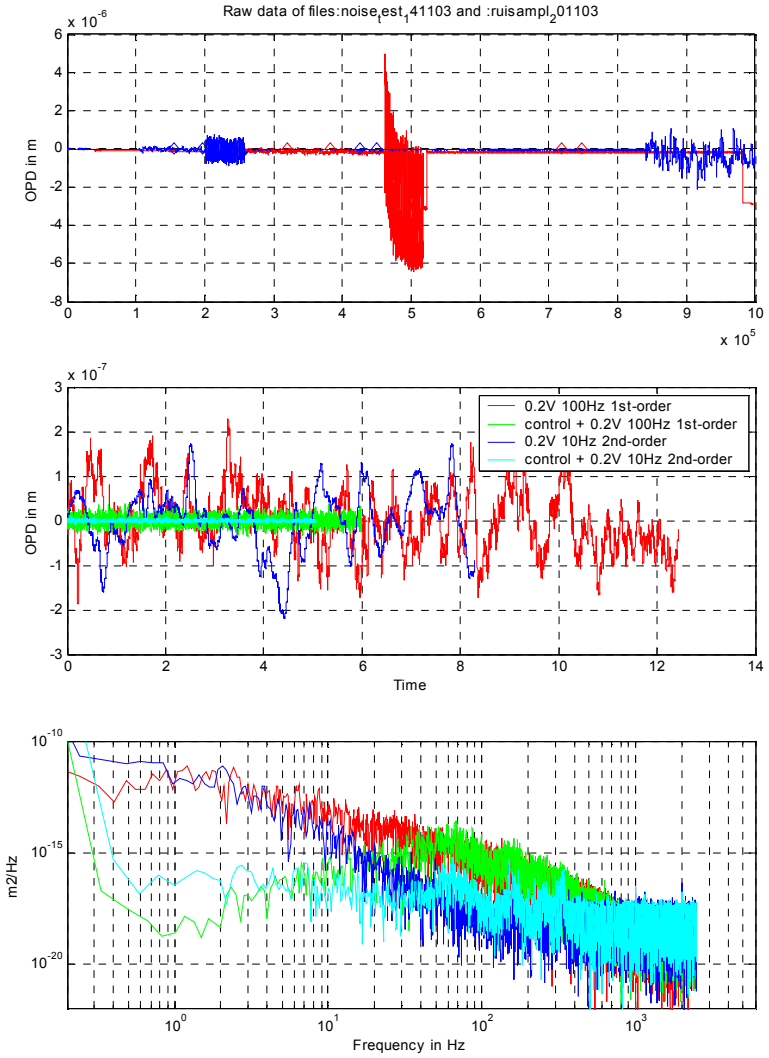

Figure 10 Effect of noise type on resulting OPD stabilisation

Two types of noise were tested, a first order drop-off noise and a second order drop-off noise. In figure 10 a comparison is made. Again the first plot shows the raw data of two files, where the diamonds indicate the selected data parts. In the second plot these selections are depicted on top of each other after subtracting the offset. Both noise types roughly show the same amplitude, but it can be observed that the 2nd-order noise has a substantial amount of high order noise. A better comparison is obtained, when observing the PSD of the noise in the third plot. Here the two noise spectra are represented by straight lines with different slopes. The slopes are equal to twice the drop off, thus 10^{-2}/decade for the first order drop-off and 10^{-4}/decade for the second order drop-off. For higher frequencies the signal is dominated by the background noise. This is around 100 Hz for the second order drop-off noise and around 700 Hz for the first order drop-off noise.

After stabilisation the resulting signals are lower for the second order drop-off noise than for the first order drop-off noise. This is due to the relatively large extend of high frequency noise in the first order drop off noise. Since the achievable reduction is roughly the same for both noise types, more noise will remain for the first order noise. As a rough approximation the noise reduction in the OPD seems to follow a second order law, decreasing the performance 100 times for every frequency increase of 10. Although other experiments indicated that the achievable noise level after stabilisation remains unaltered with increasing noise amplitudes. OPD noise reduction values up to 10^7 for low frequencies (few) have been observed.

6. CONCLUSIONS

Direct testing of the Fine Lateral Sensor (FLS) functional requirements yields good results for both the pointing stability and the sensitivity. The resulting sensitivity is better than required (10 μm/√Hz @ 10 Hz). This resolution requirement can be met at a 1kHz control frequency, or at the described 10 Hz a resolution of 0.2 μm can be achieved. When predicting the FLS performance under space temperature conditions the experiments indicates that the system should work under SMART3 conditions. This conclusion is supported by the following experimental results:

- Variations of spot shape only have is minor effect on the sensitivity and linearity.
- Pointing stability is better than required.

The OPD control works at a sufficiently high level, as was shown before in a number of other projects. Here it was identified that the reduction of noise varies with the type of noise, the noise amplitude and the applied controller:

- The resulting OPD-stabilisation is better for low frequency noise. (<10 Hz)
- The noise reduction is limited to frequencies below 50 Hz due to the poor piëzo performance (band-width).
- Both PID and IMC-controller work well under optimised conditions.
- The IMC-controller works orders of magnitude better than the PID-controller in non-optimised conditions, or where modal frequency components are present.

7. ACKNOWLEDGMENTS

This work is funded by the European Space Agency in the framework of the “High Precision Optical Metrology” contract.
EADS Astrium (France and Germany) is the prime contractor for this study with contributions from the following companies and institutes:
EADS CASA Espacio (Spain) for the experiments in vacuum
INETI (Portugal) for the design and manufacturing of the absolute distance measurement breadboard
SIOS and TU-Ilmenau (Germany) for the design and manufacturing of the heterodyne distance measurement breadboard
Humbold Universität zu Berlin (Germany) for the design and manufacturing of the frequency stabilisation breadboard

8. REFERENCES

1. B. Calvel, I. Cabeza, A. Cabral, E. Manske, J. Rebordao, R. Sesselmann, Z. Sodnik, A. Verlaan, “High Precision Optical Metrology for Darwin: Design and Performance”, 6th International Conference on Space Optics, Toulouse, April 2004.
2. H. van Brug, T. van den Dool, W. Gielissen, P. Giesen, B. Oostdijck, L. d’Arcio, “Delft Testbed Interferometer – layout design and research goals –“, *Interferometry for Optical Astronomy II*, Hawaii 2002, SPIE **Vol. 4838**, pages425-429 (2003)
3. B.Snijders, B.C. Braam, H Bokhove, “Free-beam delay line for a multi aperture optical space interferometer stabilised on a guide star”, Proc. SPIE **Vol. 2209**, p423-430, Space Optics (1994)
4. B. Snijders, P. Kappelhof, B.C. Braam, H.J.P. Vink, P. Verhoeff, “GAIA testbench: monitoring the basic angle with microarcsecond accuracy” Proc. SPIE **Vol. 4006**, p915-956, Interferometry in Optical Astronomy (2000)